M. P. Manahan, Sr.[1] and R. B. Stonesifer[2]

The Difference Between Total Absorbed Energy Measured Using An Instrumented Striker and That Obtained Using an Optical Encoder

---

Reference: Manahan, M. P., Sr., and Stonesifer, R. B., **"The Difference Between Total Absorbed Energy Measured Using An Instrumented Striker and That Obtained Using and Optical Encoder"**, *Pendulum Impact Testing: A Century of Progress, ASTM STP 1380*, T. A. Siewert and M. P. Manahan, Sr., Eds., American Society for Testing and Materials, West Conshohocken, PA, 1999.

Abstract: The application of optical encoders in Charpy impact energy measurement has improved significantly the accuracy of "dial energy" determination. Instrumented strikers offer an alternative method of energy measurement which is accurate and reproducible for both conventional and miniature specimen testing while providing additional useful information such as general yield load, peak load, brittle fracture load, and brittle fracture arrest load. It has been observed that the total absorbed energy measured using these two technologies, while generally in good agreement, sometimes differs by a significant amount. The instrumented striker total absorbed energy has been found to be higher or lower than the optical encoder energy depending on the ductility of the test specimen and other factors. This paper examines and provides explanations for these energy differences. A summary of mechanisms for pendulum energy loss, other than in fracturing the test specimen, is provided along with estimates of the amount of energy which may be associated with each mechanism.

Keywords: impact testing, instrumented striker, absorbed energy, optical encoder

Introduction

The energy measured by the dial in a Charpy test is basically the potential energy lost by the pendulum as determined from the difference in height of the pendulum's mass before and after its swing. This energy commonly is measured by either a mechanical dial gage or an electrical encoder that essentially measures the pendulum angles at the start and end of the swing. It is the energy that goes into dynamically deforming and fracturing the test specimen that is intended to be measured by the Charpy test. Energy that is lost through other mechanisms is not intended to be included in the measured Charpy energy. For example, loss due to friction of the pendulum with the surrounding

---

[1] President, MPM Technologies, Inc., 2161 Sandy Drive, State College, PA 16803.
[2] Owner, Computational Mechanics, Inc., 1430 Steele Hollow Road, Julian, PA 16844.

air and loss due to bearing friction are corrected routinely by measuring the energy loss due to swinging the pendulum without a specimen being installed in the test machine. Since it is the energy that goes into the specimen that is intended to be measured, a more direct means for measuring this energy is to measure the work that is done on the specimen by the striker during the impact. This work can be calculated if the force exerted on the specimen and the displacement at the striker contact surface is known throughout the period of contact between the striker and the specimen. It is possible to build a load cell into a Charpy striker that provides impact force as a function of time. The displacement history can be obtained by using the initial velocity at the time of first contact and the striker deceleration history. The measured force is used to compute the deceleration history of the pendulum using Newton's second law (e.g., F = ma). Two integrations of the deceleration versus time function, combined with the initial velocity, provide the required displacement function.

The impetus that led to the work reported in this paper was the observation that significant differences can sometimes exist between Charpy energies measured via the dial gage/encoder technology and those determined by calculating the work done on the specimen via the use of a striker load cell. This paper describes several opportunities for such energy differences to arise. Some of the mechanisms illustrate that the dial gage/encoder approach can result in larger energies being reported than actually go into the specimen. Other mechanisms illustrate that loads measured by striker load cells may involve some error. As should be expected, neither approach to measuring the energy to break the specimen (i.e., the Charpy energy) is perfect.

A combination of experimental and numerical studies was used in this work. The bulk of the experimental work was done using 4340 steel specimens which were provided by the National Institute of Standards and Technology (NIST). Three calibration specimen types were used, low energy (≈17 J), high energy (≈100 J), and super high energy (≈225 J), so that the entire spectrum of specimen behavior (very brittle to very ductile) could be studied. Comparing encoder-based energies to the integrated striker energies from NIST's low, high, and super high specimens, for a large number of tests, it was found:

- low energy specimens resulted in encoder energies 10-17% greater than the instrumented striker's integrated energy (2 to 3 J difference)
- high energy specimens resulted in encoder energies 2-3% less than the instrumented striker's integrated energy (3 to 4 J)
- super high energy specimens resulted in encoder energies 1-2% less than instrumented striker's integrated energy (3 to 4 J)

It can be seen that the energy differences for the low energy specimens are much larger than for either the high or super high specimens when viewed on a percentage basis. On an absolute energy difference basis, the low energy specimens have slightly less difference than the high and super high specimens. The sign of the energy difference changes as the ductility of the specimen increases.

It was also observed that the low energy specimen energy difference was dependent on whether the specimen halves exited from the front or the back of the machine. When tested at room temperature, the low energy specimens consistently exited the machine in the same direction as the swing of the striker (front). When tested at a lower temperature, the low energy specimens often exited counter to the striker swing direction (to the back).

For these rear exiting specimens, the energy difference was about 5% less than for the room temperature specimens that exited from the front. This leaves a difference of about 1 to 2 J. It was also observed that occasionally a super high energy specimen would not break into two pieces. For these specimens, the difference between encoder energy and integrated striker energy was near zero.

Three dimensional (3D) finite element simulations were performed which made use of two models. The grid for one model represented the pendulum, U-hammer, and striker of a Tinius Olsen model 84 test machine (see Figure 1). The center of percussion for this grid was within 0.25 mm (0.01 in.) of the designed center of strike (CS). The grid for the other finite element model represented just the instrumented striker portion of the hammer. The finite element model of the entire pendulum included the effect of deformations and vibrations in the pendulum assembly and was easily altered so as to determine the effect of shifting the strike location relative to the pendulum's center of percussion. The detailed finite element model of the striker was useful for comparing dynamic load cell response to static load cell calibration behavior and for studying the effects of non-uniform contact pressure distributions between the specimen and the striker. Input to these finite element models was either the force versus time history from an actual test, or an idealized impulse defined by:

$$f = F_{\max} \sin\left(\frac{\pi t}{t_t}\right) \text{ for } 0 \le t \le t_t \tag{1}$$

$$f = 0 \text{ for } t > t_t$$

By varying t_t, this idealized impulse was used to determine the effect of impulse duration (or frequency) on the load cell behavior.

Vibrational Energy in the Pendulum

The encoder-based energy gives a very reliable indication of the total energy loss in the experiment. This encoder-based energy loss includes the desired Charpy test energy as well as losses due to windage and friction (until corrected), any secondary impacts with the broken specimen, and vibrational energy that remains in the pendulum assembly. The striker energy integration, on the other hand, does not include any vibrational energy left in the pendulum, and does not reflect energy transfers between the striker and the specimen that take place after the specimen breaks. A study was made to determine if the tendency for integrated striker energies to be smaller than encoder energies for low energy specimens could be explained by vibrational energy left in the pendulum.

The full pendulum finite element model was used for this study. A series of analyses were made using an idealized impulse loading with impulse times (t_t) ranging from 2 to 5000 μsec. It was important to study such a wide range of impulse times because Fourier decomposition of Charpy load versus time histories results in a similarly wide range of frequencies. Furthermore, the pendulum vibration amplitudes and energies excited by an impact depend on the impulse duration as a result of their ability or inability to excite the pendulum's natural modes and frequencies of vibration. ASTM Standard Test Methods

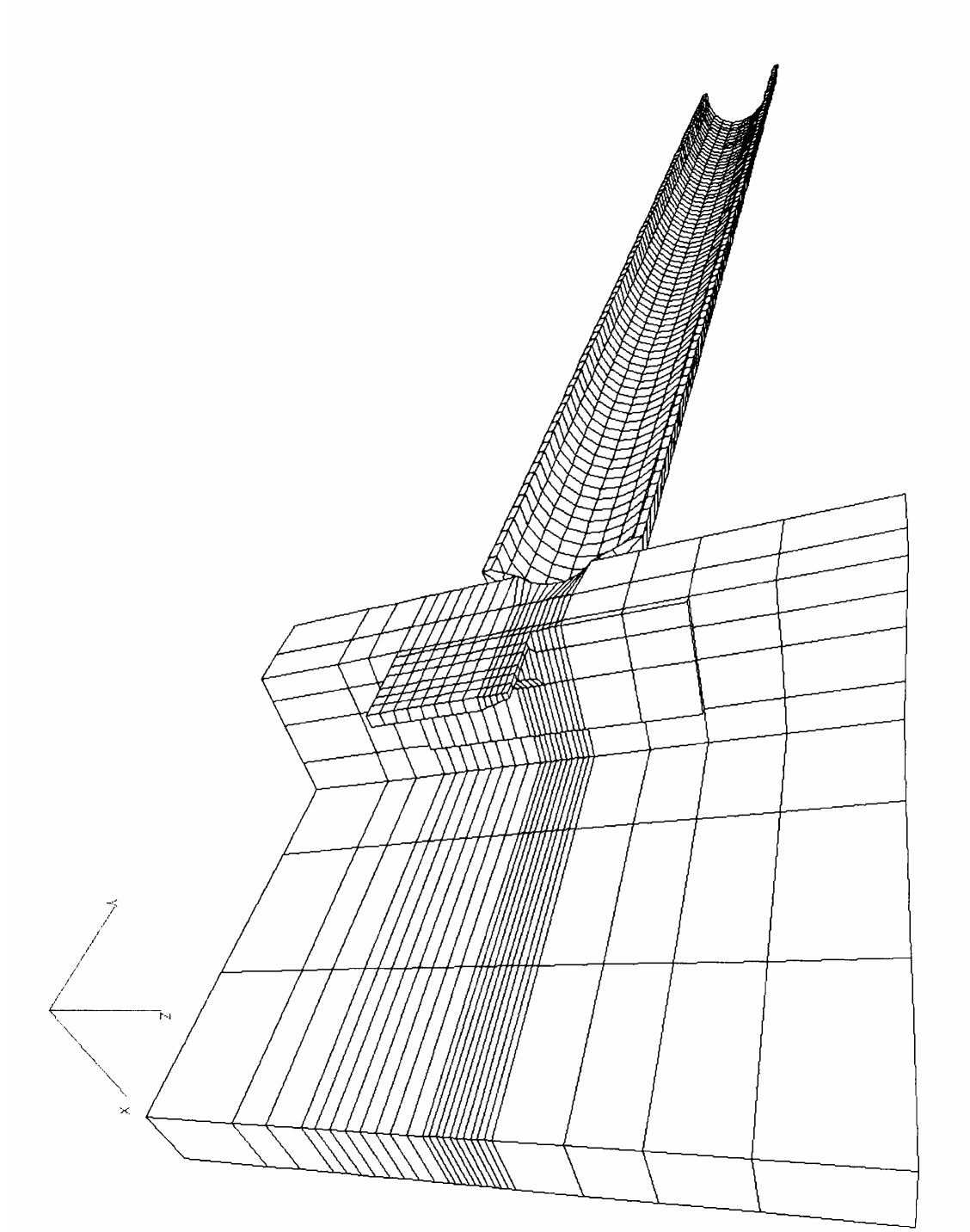

Figure 1-*Finite Element Grid of the Charpy Test Machine Pendulum*

for Notched Bar Impact Testing of Metallic Materials E23 allows Charpy test machines to have their center of percussion (CP) above or below the CS by as much as 1% of the distance between the pendulum's axis of rotation and the CS. Since shifting the strike location relative to the CP would also be expected to affect the tendency to excite vibrations in the pendulum, the finite element study considered three strike locations. One location was essentially at the CP, one was 1% (8.9 mm) above the CP, and the other was 0.57% (5.1 mm) below the CP. The lower point was not shifted the full 1% because the striker does not extend far enough to allow this. Due to assumed symmetry in the geometric modeling and impact force loading, torsional and lateral pendulum vibrations inherently were assumed not to exist.

Figure 2 shows the results of the finite element analyses which explored the effect of impulse duration and impact location on pendulum vibrational energy. The peak impact force (F_{max}) was kept constant at 620 kN (7000 lb) for all analyses. With peak force kept constant, the nominal impact energy was proportional to the impulse duration. It can be seen that the pendulum and striker vibrational energy is very dependent on both impulse duration and strike location. Figure 2a shows that the least vibrational energy (~0.05 J) is left in the pendulum for all three strike locations when impulse durations are around 250 μsec. With impacts at or below the CP, the peak vibrational energies (1.2 and 1.7 J) occurred near an impulse duration of 33 μsec. While the impacts at 1% above the CP had a local peak at 33 μsec (0.6 J), the highest computed vibrational energy was 2.9 J for an impulse duration of 5000 μsec. Figure 2b shows the same vibrational energy results as Figure 2a except that the vibrational energy is normalized by the nominal impact energy. For impulse durations of 250 μsec or larger, the vibrational energy in the pendulum that remains after the impact is 0.2% or less of the total impact energy. However, for impulse durations of less than 250 μsec, the portion of the impact energy that goes into pendulum vibrational energy continually increases until 100% is approached for about a 2 μsec duration.

Based on the results of Figure 2, it is concluded that while ductile specimens, such as the NIST high and super high materials, might be expected to induce as much as 3 J of pendulum vibrational energy, this energy is negligible compared to the total Charpy energy being measured. On the other hand, for the NIST low energy material, the total impact duration is about 200 μsec. It therefore appears from Figure 2 that vibrational energy should be near zero both in absolute and relative terms. However, one must recall that the impulses used in this study were smooth idealized impulses. While the total impact duration of the low energy specimens may be 200 μsec, the effect of the rapid load decrease due to brittle fracture is more accurately represented by idealized impulses of 10 to 40 μsec duration. For these impulse durations, vibrational energies in the 0.5 to 1.5 J range are expected. This explains most of the observed difference for low energy specimens which exit the back of the test machine.

Pendulum vibrational energies were computed for finite element simulations in which force histories from each of the three NIST specimen types were used as input. With impact at the CP, the vibrational energy left after impact was 0.26 J, 0.41 J, and 0.64 J for the low, high, and super high specimens, respectively. These results are reasonably consistent with the results of Figure 2. Impacting at 1% above the CP led to 0.14 J, 0.77 J, and 1.4 J, respectively, and as predicted in Figure 2, the low energy specimen

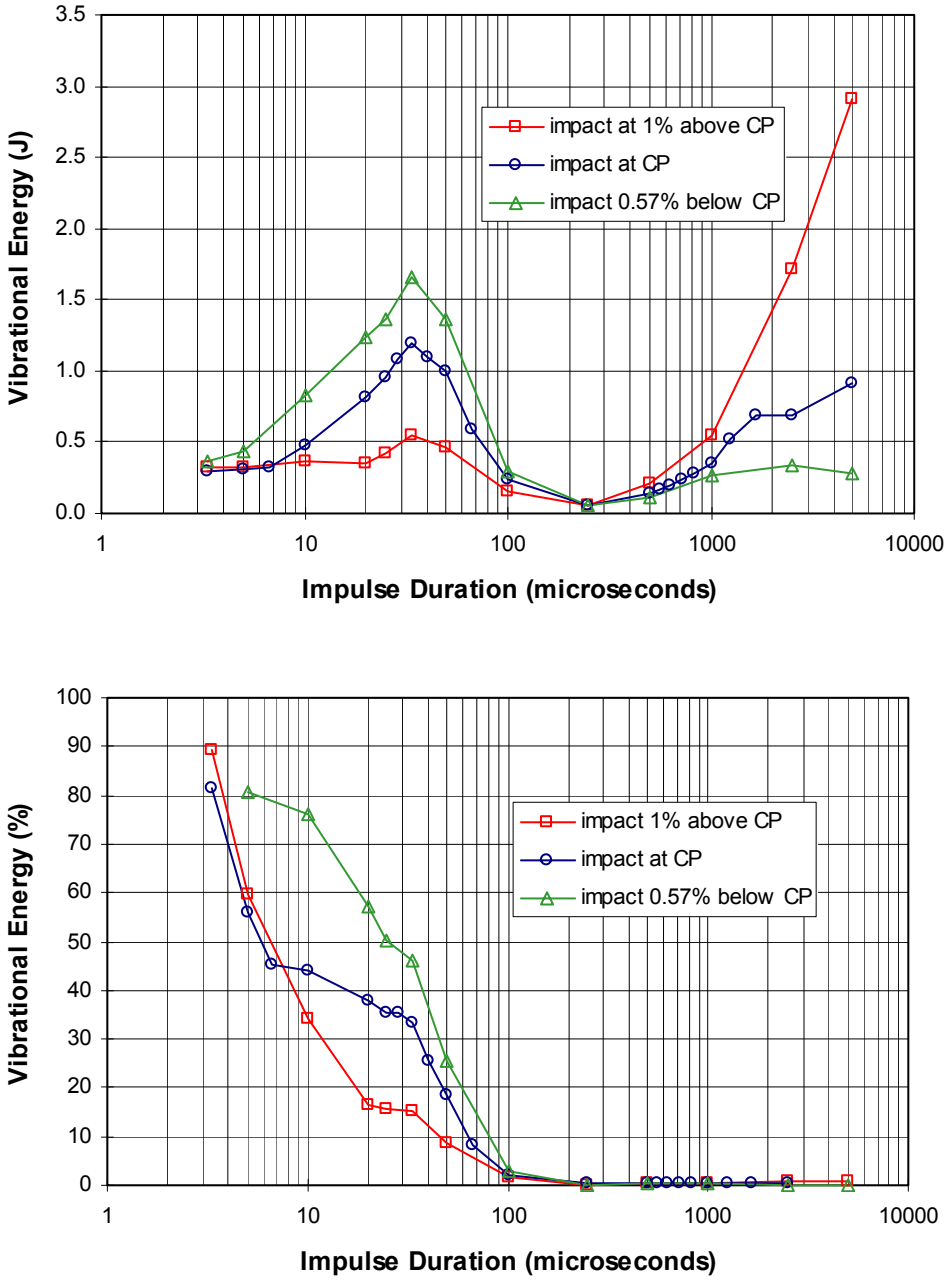

Figure 2-*Pendulum Vibrational Energies for Various Impulses and Strike Locations (Fmax =620 kN) (top) Vibration Energy Magnitude Versus Impulse Duration (bottom) Normalized Vibration Energy Versus Impulse Duration*

vibrational energy decreased while the other two increased. It was found that artificially shortening the unloading time associated with the brittle fracture of the low energy specimen (5 μsec instead of 20 μsec) raised the vibrational energy from 0.26 J to 0.44 J.

It was concluded that the pendulum vibrational energy is an important factor in the observed encoder versus striker energy differences. The finite element simulations showed that the pendulum vibrational energy effect typically increases the encoder based energy relative to the integrated striker energy by 0 to 1 J, but could perhaps increase the energy by as much as 2 J in some cases. This effect therefore helps to explain the observed 2 to 3 J difference between the encoder and integrated energies for the brittle specimens, but cannot explain the entire difference. The vibrational energy effect does not help to explain the observed energy differences for the more ductile specimens since for those specimens the integrated energy is larger than the encoder-based energy. Further, most of the vibrational energy for a ductile specimen is transferred from the hammer to the specimen as a result of plasticity damping.

Striker Calibration

Calibration of the striker load cell is done using a static loading. Therefore, it is assumed inherently that static loading of the striker results in similar strains in the striker as dynamic loading. Using finite element simulations, it was shown that inertial effects would not significantly reduce the load cell accuracy even for such dynamic events as unloading due to brittle fracture and ringing of the specimen during initial loading. This section addressed the effect of changes in contact pressure distribution on the striker. Questions of interest included:

- How sensitive is the load cell to contact pressure distribution?
- Do geometric imperfections of specimens that meet ASTM E23 lead to significant differences in the contact pressure distribution?
- Do deformations of the striker and pendulum assembly lead to significant differences in the contact pressure distribution?
- Do large specimen deformations lead to significant differences in contact pressure distribution as a result of pendulum rotation?
- Does pinching of the striker tip by very ductile specimens alter the indicated load?
- How sensitive is the load cell calibration to alignment of the calibration load frame?

Initially, contact with the specimen is limited to the center line of the striker contact surface. As the specimen deforms, the contact pressures become more evenly spread over the contacting surface. For very ductile specimens, the corners of the ASTM E23 standard striker contact surface can embed themselves in the specimen to the extent that further bending of the specimen causes a pinching of the leading edge of the striker. This range of potential contact pressure configurations was simulated by three idealized contact pressure distributions. The first was for a line contact at the striker centerline that extends the entire specimen height. The second was for a uniform pressure over the entire nominal contact region. The third was for two lines of contact at the outer edges of the contacting surface.

Forces for this first part of the contact pressure study were uniform with regard to vertical position on the contacting surface. It was found that the indicated load was less

than the applied load by 0.4%. The indicated load was larger than the applied load by 0.8% when the uniform contact pressures were replaced by forces concentrated at the edges. The static calibration is performed with a specially machined and hardened calibration specimen. Due to the lack of plasticity in the calibration specimen, the contact pressures during calibration are largely concentrated near the striker contact surface centerline. This means that the calibration is most applicable to specimens with little plasticity before fracture. The indicated load error for a very ductile specimen then would be less than 1.2%. The trend for larger indicated forces with more ductile behavior is consistent with the observed differences between encoder-based energy and integrated energies from the striker force history (an error in load cell indicated force results in a nearly proportionate error in the integrated energy). A 1.2% indicated load error for the high energy specimens would lead to a 1 to 2 J energy error. A 1.2% indicated load error for the super high energy specimens would lead to a 2 to 3 J energy error. These estimated upper bound energy errors are slightly smaller than the 3 to 4 J difference noted above for high and super high specimens.

The next phase of the contact pressure distribution study examined the effect of force variations in the vertical contact surface direction (along the striker surface parallel to the notch). Such variations can arise from many sources, including: non-square specimen cross-section; elastic deformation of the striker due to the impact load; elastic bending of the pendulum due to the impact load; rotation of the pendulum during a ductile test; and misalignment and imperfect machine geometry. The ASTM E23 test standard states that the machining tolerance for specimen squareness is 10 minutes for adjacent sides. The striking edge is to be parallel to a perfectly square specimen to within 1:1000 (3.4 minutes). The anvil is to be perpendicular to the specimen support to within 9 minutes.

The finite element model of Figure 1 was used to compute rotation of the striker contact surface during numerous impulse loadings. Figure 3 summarizes the contact surface rotational behavior as a function of the impulse duration. The peak force was 620 kN (7000 lb) for all analyses. A static load of 620 kN was found to induce a 0.0022 radian (0.13 degrees or 8 minutes) rotation of the contacting surface due to elastic shear and bending deformation in the striker. This 8 minute rotation due to striker deformation is comparable to the ASTM E23 specimen machining tolerance of 10 minutes. Positive rotations were arbitrarily defined so as to promote loss of contact at the bottom of the contact region. For the very shortest impulse loadings, inertial effects limited the rotation of the contact surface. For impulse durations between 20 and 100 μsec, the contact surface rotations were found to be comparable in magnitude to those from a static loading and are again primarily due to local elastic deformation of the striker. For impulse durations greater than about 200 μsec, the contact surface rotation due to the overall rotation of the pendulum is larger than the rotation due to local elastic deformation of the striker. For the longest impulse load duration of 5000 μsec, the pendulum rotation is about -0.03 radians (1.7 degree or 100 minutes). This is about 14 times the rotation due to striker deformation and is opposite in direction. The low energy specimens have a total impulse time between 100 and 200 μsec, while the high and super high energy specimens have impulse durations between 3000 and 5000 μsec.

The range of striker contact region rotation due to local deformation (indicated by curves with circular and triangular points in Figure 3) reflects the dependence of the

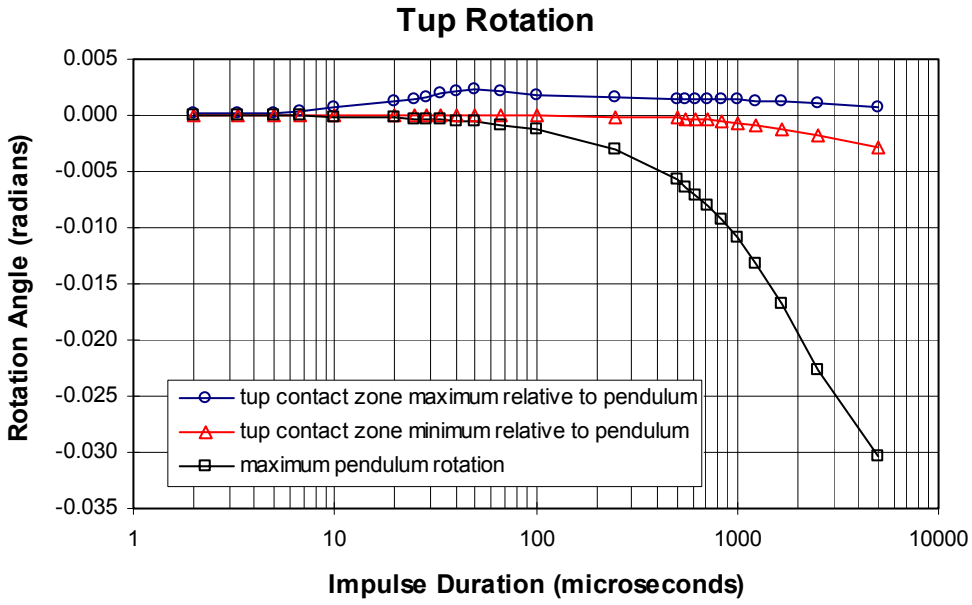

Figure 3-*Striker Contact Surface Rotation Due to Impulse Loads of Various Duration (Fmax = 620 kN)*

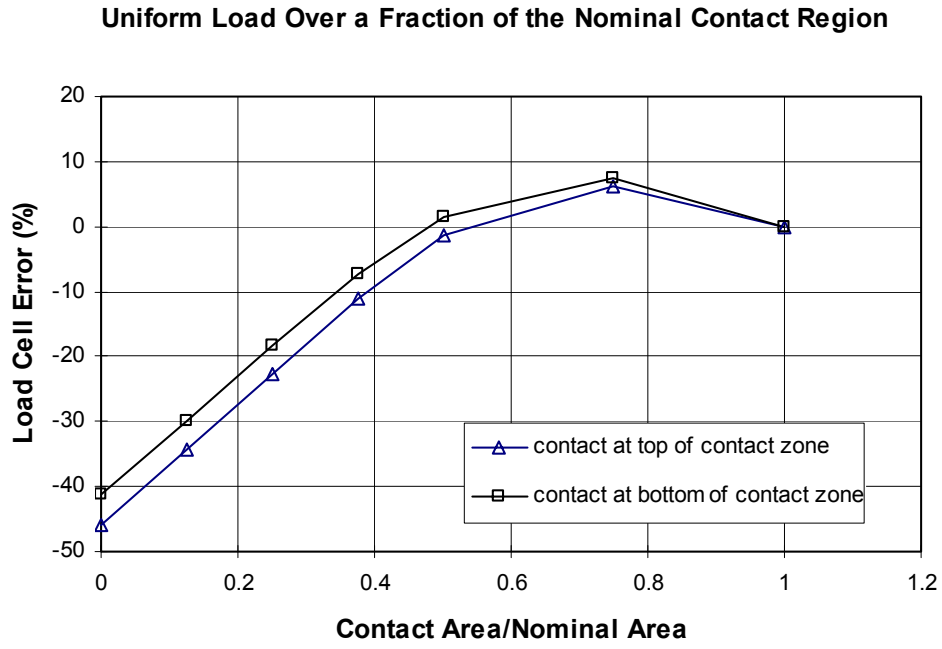

Figure 4-*Striker Load Cell Error Due to Uniform Contact Pressure Distributions that Cover Less than the Full Nominal Striker Contact Region*

rotations on time. It was found that the dynamic rotations could not be correlated with those for static loading based on instantaneous load levels. This means that inertial effects on rotation behavior are significant and that any effect of rotations on dynamic load cell behavior will not be automatically corrected by rotations that occurred during the static calibration procedure. Due to the effect of contact surface rotations on load cell behavior, it was considered necessary to assess the effect that force distribution variations, such as might be induced by striker contact surface rotations, would have on load cell accuracy.

The baseline contact pressure distribution was a uniform contact pressure over the entire nominal contact area. Two types of contact pressure variations were simulated with the detailed striker finite element model. The first was a linearly varying distribution that covered the entire nominal contact region. The pressure was maximum at either the top or bottom edge of the contact zone and decreased linearly to zero at the opposite edge. The second variation simulated a uniform pressure distribution that covered only a portion of the nominal contact region. For this case, the contact region width was varied from a line contact at either the top or bottom edge to a case with contact over 75% of the nominal contact region. It was found that the linear distribution cases covering the entire nominal contact region resulted in an indicated load about 1% above the actual load when the peak pressure was at the bottom of the contact region and resulted in an indicated load about 1% below the actual load when the peak pressure was at the top of the contact region. By linear superposition of these linear pressure distributions with the baseline uniform pressure case, it can be concluded that any linear pressure distribution will result in load cell accuracy of 1% or better.

Figure 4 shows the results of the load cell simulations that considered the effect of uniform contact pressures existing over a portion of the full nominal contact region. This type of distribution is representative of behavior in which loss of contact occurs at either the top or bottom edge of the striker but plasticity in the specimen limits the peak contact pressure and distributes the contact force over a finite area. The baseline contact behavior (uniform pressure over entire nominal contact region) is represented by the common point at the right ends of the two curves. Surprisingly, for the case in which the contact region covers 75% of the nominal contact area, the indicated loads are 6 to 8% above the actual applied load. For the case in which the contact region covers 50% of the nominal contact region, the indicated loads are within 1.5% of the actual load. The errors increase in magnitude as the contact regions are further reduced, with errors for line contacts at the top and bottom edges of the nominal contact region being -46 and -41%. The limiting case of a line load will not be reached for a real specimen since plasticity tends to spread the load over a finite width region.

The tendency in Figure 4 for indicated loads to be larger than actual loads for contact areas larger than 50% and smaller than actual loads for the areas less than 50% could help to explain the observed differences between encoder-based energy and the integrated energy. Loss of contact due to contact surface rotation would be expected to be more dramatic (i.e., smaller contact area) for specimens exhibiting little plasticity. The behavior of Figure 4 would therefore be consistent with the observed differences if the low energy specimens had effective contact areas less than 50% and the higher energy specimens had effective contact areas greater than 50%.

As described above, since contact pressure distributions and rotations of the contact surface can have a significant effect on the load cell behavior, static calibration procedures should produce similar behavior as the dynamic loading that occurs during testing. The striker load cell was found to be relatively insensitive to lateral pressure distribution variations and therefore, it was concluded that calibration procedures could use a carefully machined and hardened calibration specimen that tends to concentrate loads at the striker centerline. In applying loads to the striker during static calibration, much care must be taken that the applied loads are aligned with the striker contact region. Any offset results in differences between the applied load and the striker reaction force due to reaction forces at the pendulum's axis of rotation. Perhaps even more importantly, however, is that an offset will affect the amount of contact surface rotation and thus the contact pressure distribution. A numerical simulation found that applying a calibration force to the hammer at 44.5 mm above the CS led to a difference in applied force and striker reaction force of 5.2% and increased the contact surface rotation by a factor of 4.6 (34 minutes instead of than 8 minutes). Applying the force at 13 mm below the CS resulted in a 1.5% force difference and the contact surface rotation was -2 minutes (direction reversed from perfectly aligned calibration force). It was concluded that control of the applied calibration force location to within 3 mm of the CS results in applied force errors and additional contact surface rotations that are tolerable.

Energy Integration

The force versus time record obtained by the instrumented striker can be used to compute work done on the specimen only if the specimen displacement is also known. Displacements can be calculated if the pendulum velocity at the instant of first contact with the specimen is known. This is done by using the measured force to compute the deceleration history via Newton's second law ($a = F/m$), integrating the deceleration to get the velocity history, and then integrating again to get displacements. The initial velocity enters as a constant of integration. The initial velocity is obtained by equating the kinetic energy just before impact to the initial potential energy of the pendulum less a windage and friction correction ($\frac{1}{2} mv^2 = mgh - E_w - E_f$) and solving for velocity. This procedure involves two assumptions. It is inherently assumed that the pendulum and striker are rigid since displacement at the specimen contact is assumed to be the same as that at the pendulum's CS. The second assumption is that the pendulum is struck at its CP.

Striking the pendulum at the CP makes the mechanics equations relating impact force, pendulum deceleration, velocity, and kinetic energy very convenient since the equations reduce to those for a point mass (as outlined above). The mass that is used in these simplified equations is a pseudomass (not the true mass). It is measured by weighing the pendulum at its CP while the pendulum is horizontal and supported at its pivot point. If the impact is not at the CP, the simplified equations begin to entail some error since it is then necessary to consider mass moments of inertia (I) and angular velocities. The magnitudes of the errors associated with using the simpler equations are governed by the ratio r_{cs}/r_{cp} , where r_{cs} is the distance from the axis of rotation to the CS and r_{cp} is the distance from the axis of rotation to the CP. The ASTM E23 standard states that this

ratio must be between 0.99 and 1.01. A study was done to assess the effect of not having a rigid pendulum and striker and of having the CS different from the CP.

Interestingly, it was found that while many of the mechanics relations are affected by not having the CS at the CP, the relationship between pendulum angles before and after strike and the total energy loss remains perfectly accurate provided the pseudomass is obtained by weighing the pendulum at its CS and not at its true CP. The initial impact velocity on the other hand is affected by not striking at the CP. The actual initial velocity is $\sqrt{r_{cs}/r_{cp}}$ times the initial velocity resulting from application of the simple equations. Due to the square root and the ASTM E23 ±1% limitation on r_{cs}/r_{cp}, the maximum initial velocity error associated with use of the simple equations is 0.5%. The actual deceleration of the pendulum is equal to r_{cs}/r_{cp} times the deceleration resulting from application of the simple equation ($F = ma$). Since initial velocity and accelerations are affected by r_{cs}/r_{cp} not being equal to unity, the energy resulting from integration of the instrumented striker force data will also be affected.

The effect of the r_{cs}/r_{cp} corrections on Charpy energies obtained by integrating striker force data is to increase the computed energy if striking below the center of percussion and to decrease the computed energy if striking above the center of percussion. The effect of the acceleration correction is to offset the effect of the velocity correction. Since the acceleration correction is smallest for low energy specimens, the largest integrated energy error is found for low energy specimens. Through numerical experimentation, it was found that if the CS is within 1% of the CP, the upper bound energy error associated with using the simple equations would be 0.5%. However, since the locations of the CS and CP can be easily determined, the above velocity and acceleration corrections can be applied and even this small error can be avoided.

Next, a study was made to determine the effect of striker and pendulum deformations on the displacements used in the energy integration. Finite element calculations showed that actual dynamic striker contact surface displacements could differ from idealized rigid body displacements by as much as 10 to 20% (see Figure 5). It can be seen from Figure 5 that the displacement difference reaches a maximum near peak load and then decreases to zero as the load decreases. A load versus displacement behavior that results from correcting the rigid pendulum displacements with deformations based on stiffness from a static finite element analysis is shown in Figure 5. It can be seen that the correction based on static deformation behavior tended to be too large compared to displacements from a dynamic finite element simulation. More importantly, however, it was found that the static displacement correction made no difference in the total integrated energy. This is due to the correction displacement being precisely proportional to the load. When actual dynamic finite element displacements were used in the energy integration, there was an effect on the integrated energy. Therefore it can be concluded that this energy effect of deformation related displacements is entirely due to inertial effects. It was found that using the idealized rigid pendulum displacements always led to the integrated energy being larger than if actual dynamic displacements were used. Table 1 shows the increase in integrated energy that resulted when the idealized rigid pendulum displacements were used instead of actual dynamic

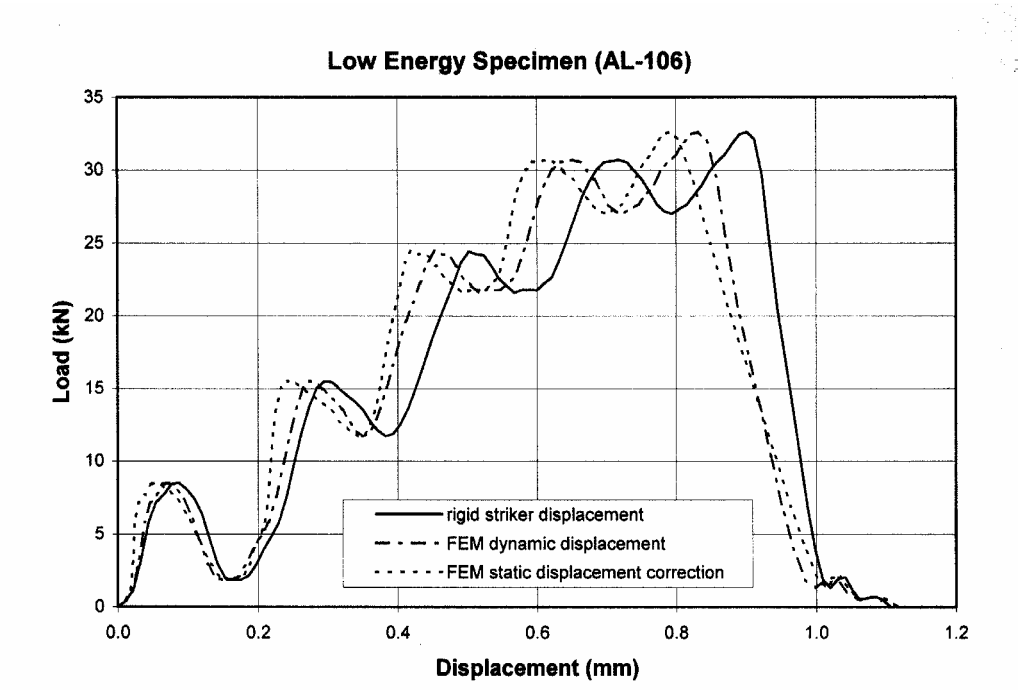

Figure 5-*Effect of Pendulum and Striker Deformation on Specimen Load versus Displacement History*

Table 1-*Additional Integrated Energy when the Striker and Pendulum are Assumed to be Rigid*

Specimen	Strike Location	Energy Error near Peak Load (J)	Energy Error for Entire Test (J)
AL-106	0.2” below CP	1.1	0.5
AL-106	at CP	1.2	0.4
AL-106	0.35” above CP	0.8	0.4
AH-147	0.2” below CP	1.2	0.8
AH-147	at CP	1.2	0.8
AH-147	0.35” above CP	1.0	1.5
SH-398	0.2” below CP	1.8	1.3
SH-398	at CP	1.8	1.3
SH-398	0.35” above CP	1.3	2.4

displacements. Energy effects of using rigid body displacements in the integration range from about 0.5 J to 2.5 J, with higher energy specimens having the higher energy differences. Except for higher energy specimens with impact significantly above the CP, the energy difference around peak load is larger than the final energy difference. While the static deformation correction did not affect the overall integrated energy, it did result in a difference for energies up to peak load. Therefore, the static deformation energy correction could be useful if the total energy is to be partitioned.

Work at the Bearing

Energy loss at the bearing can be of two forms. The frictional loss is commonly corrected along with windage loss. Bearing friction and windage loss are reasonably determined by measuring the losses during a swing of the pendulum without a specimen and then scaling the loss based on the ratio of the swing arc during an actual test to that from the free swing arc. Losses also can occur as the result of radial play at the bearings. This second type of energy loss will not occur during a free swing because there are no vibrations in the pendulum. Theoretically, if the pendulum was rigid and the impact was at the pendulum's CP, still there would be no loss at the bearings due to radial play since no forces would be generated at the bearing. However, the pendulum is not rigid, and significant forces can be generated at the bearing due to the impact even if the impact is at the CP. Finite element simulations have found vibrational bearing reactions in the 0.4 to 2 kN range. This range of forces acting through the ASTM E23 maximum allowable radial play of 0.075 mm gives an energy dissipation of 0.03 J to 0.15 J. Since this force is cyclic, each cycle will involve additional energy loss. A 4000 μsec test (representative of super high energy specimens) might involve as many as two full cycles at the bearing thus resulting in four times the above energies being dissipated (0.12 J to 0.6 J). A low energy specimen test takes so little time that less than half a cycle occurs, and thus the above energies (based on a half cycle) would be reduced. These energy losses are conservative if bearing radial play is less than the allowable. These energy losses would be included in the Charpy energy if the encoder was being used. Obtaining Charpy energy from integrating forces from an instrumented striker would not include the bearing related energy loss.

Geometry Effects

Imperfect specimen geometry or imperfect specimen position is generally expected to result in more opportunity for secondary impacts between the broken specimen halves and the pendulum. Any such secondary impacts will affect the encoder energy, but will not affect the energy integrated from the striker load cell. Significantly improved agreement between encoder and striker energies was found in the present study when the broken specimen halves were ejected from the rear (counter to striker motion) rather than from the front. It is believed that the rear ejection path was accompanied by fewer and perhaps no secondary strikes. The fact that there was significantly less scatter in the encoder energies for the rear ejected specimens tends to support this conjecture.

Specimen Kinetic Energy

Kinetic energy of the broken specimen is a part of the Charpy energy and will be reflected in both encoder energy and integrated striker based energies. However, the kinetic energy in the broken specimen may result indirectly in energy differences between the encoder energy and the integrated energy due to the tendency for a more energetic specimen to have more secondary impacts with the pendulum. The amount of kinetic energy that is left in a specimen after fracture is affected by three factors. The first is the amount of strain energy stored in the specimen, anvils, and striker just before fracture. The second is the speed of the striker at the onset of fracture, and the third is the amount of energy absorbed by the fracture process.

Finite element simulations show that 4 to 7 J of strain energy exist in a standard steel specimen for loads in the 23 to 31 kN range. The stored strain energy is proportional to the square of the load at fracture. Strain energy in the pendulum is about 1 J. Although not computed, strain energy in the anvils is probably no more than 1 J. All of this strain energy (5 to 9 J) is available for conversion into specimen kinetic energy upon fracture, but, as in most energy conversion processes, the conversion is not 100% efficient. As addressed above, much of the strain energy in the pendulum remains in the pendulum as vibrational energy. This probably also is the case for the anvil. The strain energy in the specimen just prior to fracture gets converted into translational kinetic energy, rotational kinetic energy, vibrational energy, and heat energy (due to fracture processes, plasticity, and friction).

The speed of the pendulum at fracture affects specimen kinetic energy since the central portion of the specimen is going at the same speed as the pendulum just before fracture. Since low energy specimens slow the pendulum the least, the speed transfer effect is greatest for the low energy specimens. The kinetic energy imparted by this transfer of pendulum speed to the specimen depends on whether the specimen breaks. If the specimen breaks and no spring action due to the release of strain energy is included (i.e., coefficient of restitution is zero), the combined kinetic energy of the specimen halves was estimated to be less than 0.2 J. If the specimen does not break and no spring action is considered, the estimated specimen kinetic energy increases to 0.6 J. A coefficient of restitution of 1 (elastic impact) results in the final specimen velocity being about twice the pendulum velocity thus resulting in the 0.2 and 0.6 J values increasing to 0.7 J and 2.6 J. The tossing energy experiments of Chandavale and Dutta [*1*] that used prebent specimens to measure energy loss associated with tossing unbroken specimens found an energy of 1.9 J. This value implies a coefficient of restitution of about 0.57 which means that about 1.5 J of the total loss was transferred to the specimen as kinetic energy and 0.4 J was dissipated via other mechanisms (e.g., heat, vibration). This experiment is therefore consistent with the above estimated specimen kinetic energy range of 0.6 to 2.6 J. It should be noted however, that the tossing energy experiments of [*1*] do not involve the large amounts of stored strain energy that exists in a real Charpy test (there being no reactions from the anvils) and therefore the measured tossing energies are probably the lower bound of tossing energies for actual tests.

The energy absorbed by fracture is believed to have the most significant effect on the specimen kinetic energy since energy absorbed by fracture processes is not available for conversion to kinetic energy. For a very low energy specimen, the energy absorbed by the fracture process has been estimated to be less than 1 J. This is just a small portion of the 5 to 9 J of strain energy that was identified above, and therefore the potential for large kinetic energies is high. For example, if 5 J of strain energy is converted into pure translational specimen kinetic energy, the specimen halves would have a velocity of 15.2 m/sec (about 2.8 times the pendulum velocity prior to impact). For very ductile specimens, the potential for energy loss due to plasticity essentially is unlimited. Specimen velocities in this case are limited largely to the pendulum velocities at the end of the fracture event.

Summary and Conclusions

The impetus behind this study was that low energy Charpy specimens resulted in encoder energies 2 to 3 J greater than the instrumented striker's integrated energy, while high and super high energy specimens resulted in encoder energies 3 to 4 J less than the instrumented striker's integrated energy. It is concluded that the observed differences between the encoder and striker integrated energies are due to a combination of factors. Table 2 summarizes the findings of this study in terms of six phenomena. The extent to which each affects the Charpy energy is summarized, and the extent to which each phenomenon is consistent with the observed experimental behavior is noted. The results have shown that the observed differences in energies are due primarily to a combination of the first four phenomena (vibrational energy, secondary impacts, partial loss of specimen contact through its effect on load cell accuracy, and pendulum deformation through its effect on displacements used in the integrated energy). The order given in Table 2 is believed to be the order of significance for the lower energy specimens. For the high and super high energy specimens, it seems likely that the pendulum deformation and partial loss of contact phenomena may be more important than secondary impacts and vibrational energy.

Reference

[1] Chandavale, R. G. and Dutta, T., "Correction of Charpy Impact Values for Kinetic Energy of Test Specimens", Pendulum Impact Machines Procedures and Specimens for Verification, ASTM STP 1248, T. A. Siewert and K. Schmieder, Eds., American Society for Testing and Materials, Philadelphia, PA.

Acknowledgments

The authors are grateful to NIST for providing the test specimens used in this study.

Table 2 -*Summary of Charpy Energy Effects*

phenomenon	energy effect	notes
vibrational energy	• can add 0.5 to 1.5 J to encoder energy • does not affect striker integrated energy	• most significant for low energy specimens • partially explains observed energy difference for low energy specimens • is not consistent with observed energy difference for high energy specimens
secondary impacts	• can add 0.5 to 1 J to encoder energy • does not affect striker integrated energy	• most significant for low energy specimens • partially explains observed energy difference for low energy specimen • is not consistent with observed energy difference for high energy specimen
pendulum deformation	• no direct effect on encoder energy • 0.5 to 1 J increase in integrated energy due to rigid pendulum assumption	• 2% (~0.5 J) error for low energy specimens • 0.5% error (~1 J) for high and super high energy specimens • consistent with observed difference for high and super high energy specimens
contact surface rotation/ separation	• no effect on encoder energy • as much as -20% to +8% error in striker loads	• <50% loss of contact leads to higher indicated load • >50% loss of contact leads to lower indicated load • may be consistent with observed energy differences for both low and high energy specimens
CP not at CS	• no direct effect on encoder energy • <0.5% error on striker integrated energy	• not a significant factor in current experiments since CS very near CP • increases vibrational energy effects
work at bearing	• < 0.5% error in encoder energy • no effect on striker integrated energy	• based on maximum ASTM E23 radial bearing play and peak vibrational forces at the bearing from finite element analyses with CS not at CP